

# A Waveguide Horn Antenna with Coupled Resonator Notch Filter Designed by the Lagrangian Formulation for Metamaterials

Joshua W. Shehan\* and Ryan S. Adams

**Abstract**—This paper presents the design and analysis of guided wave notch filters using the Lagrangian formulation for metamaterials. It is shown that the application of the Lagrangian is a convenient and effective way to select an appropriate filtering structure and determine the necessary configuration for desired filter performance. A WR-187 waveguide horn antenna is investigated with notch filters composed of broadside coupled and gap coupled split ring resonators. It is shown that broadside coupling offers significant tunability in a compact size. The filter exhibits an operational bandwidth from approximately 3.9–5.7 GHz with 40–150 MHz of instantaneous bandwidth. The fabrication of the horn antenna and split ring resonators is presented along with simulated and measured data that confirms the approach.

## 1. INTRODUCTION

Metamaterials research continues to progress due to the ability to control the propagation of electromagnetic energy in unique ways [1–6]. Metamaterials have the ability to realize effective material parameters whereby electrically small resonant scatterers can give very high, very low, and even negative effective permeability or permittivity. A key characteristic of metamaterials where the effective material exhibits either  $-\mu$  or  $-\epsilon$  is that no energy can flow through the material resulting in a stop band that can be utilized to achieve effective filtering [5–11]. The response of a metamaterial structure is commonly high- $Q$  and narrow band resulting in notch band performance. However, as the frequency spectrum becomes more crowded, there is an increasing need for narrow band notch and band reject filters for interference mitigation.

Waveguide filters are generally desirable for their low-loss, high performance, and power handling capabilities. Unfortunately, waveguide filters are generally bulky requiring large amounts of real estate. As an alternative to traditional waveguide filter approaches, there has recently been significant interest in metamaterial based approaches where considerable size reduction can be achieved using electrically small metamaterial structures. Based on the effective medium approximation where a metamaterial unit cell exhibits  $-\mu$  or  $-\epsilon$ , these electrically small resonators can be placed inside of guiding structures to realize stop band performance. The authors of [7] present a dual band notch filter using split ring resonators (SRRs) in WR-90 waveguide where the resonators are collocated for compact size. In [8], the authors demonstrate the reduction of spurious modes in a waveguide using metamaterial based filters comprised of a different unit cell. The authors of [9] demonstrate the horn antenna with a fixed frequency filter comprised of a split ring resonator at X-band. In [10], the same authors present a variation of the filter in [9] with some bandwidth enhancement. The concept for a horn antenna with an integrated tunable notch filter designed for operation at X-band is proposed in [11].

---

*Received 25 April 2016, Accepted 10 July 2016, Scheduled 21 July 2016*

\* Corresponding author: Joshua W. Shehan (jshehan@uncc.edu).

The authors are with the Department of Electrical and Computer Engineering, University of North Carolina at Charlotte, USA.

One of the challenges with metamaterial based filtering approaches is that it can be difficult to design the filters based on equivalent circuit approximations especially when coupling effects need to be taken into account. Furthermore, the filtering approaches discussed previously do not present a detailed method for reconfiguring or tuning the filter for a different center frequency without a redesign of the unit cell except for the work in [11]. In this paper, we present a notch filter design approach for coupled resonator filters using the Lagrangian formalism for metamaterials. We show that, depending on their orientation, coupled resonators can give a high degree of tunability based on manipulation of the electric and magnetic coupling parameters. As a result, the response of the filter can be tuned over wide bandwidths without a redesign of the fundamental resonant structures that make up the filter. The formulation presented herein is an extension of the work presented in [11] which marked the first account where a Lagrangian formulation was applied to guided wave filter design. Unfortunately, the drawback to the standard Lagrangian approach is that image theory must be applied to take into account coupling near metallic structures such as the walls of a waveguide. Here, we present the use of field terms in the Lagrangian where the analysis can be performed without the need for image theory creating a robust design method that can be applied to any guided wave structure.

A WR-187 waveguide horn antenna with two distinct notch filter configurations is also investigated. Gap coupled and broadside coupled split ring resonators are considered where the relative spacing between the rings is varied to tune the resonant frequency. It is shown that broadside coupling offers tremendous advantages over gap coupling in terms of tunability. We also use the coupling parameters to investigate the rejection of the broadside coupled filter over the tuning range. Numerical simulations of the radiation patterns confirm that the filtering element exhibits minimal impact to the antenna outside of the operating band of the filter. As a result, a compact solution can be realized by placing the filtering element very close to the throat of the antenna where the waveguide walls begin to flare out forming the horn. The horn antenna with three fixed broadside coupled filters is fabricated and measured; measured results confirm simulations and the design approach.

## 2. LAGRANGIAN FORMALISM AND APPLICATION TO GUIDING STRUCTURES

The most important design parameter for a notch filter of any type is the location of the resonant frequency. In metamaterial approaches, determination of the resonant frequency can be particularly challenging when coupling effects need to be taken into account. The Lagrangian formulation for metamaterials is used in several accounts to investigate the effects of coupling between structures forming bulk metamaterials [12–14]. For electrically small resonant structures, the quasi-static assumption can be applied for the response of the resonator at its lowest order mode, and the resonant dynamics of the structure are well approximated as a driven harmonic oscillator. The Lagrangian is applied under this assumption where the resonant frequency is determined based on the coupling coefficients calculated from the self and mutual energies. This is similar to coupled mode theory [15] where the Lagrangian formulation acts as a means for easily calculating the coupling parameters and backing out the resonant frequencies.

Resonant frequencies for two closely spaced metamaterial structures such as the two split ring resonators in Figure 1(a) are derived from the Lagrangian formulation as the result of two driven harmonic oscillators. The driving functions are dependent on the electric and magnetic coupling parameters,  $\beta$  and  $\alpha$  respectively [12]. The resonant frequencies for two resonators in the presence of coupling can be written as

$$f_1 = \sqrt{\frac{f_{0_1}^2 Q_1 + \beta_{12} D f_{0_1} f_{0_2} Q_2}{Q_1 + \alpha_{12} D Q_2}} \quad (1)$$

and

$$f_2 = \sqrt{\frac{f_{0_2}^2 Q_2 + (f_{0_1} f_{0_2} / D) \beta_{21} Q_1}{Q_2 + (1/D) \alpha_{21} D Q_1}} \quad (2)$$

where  $f_1$  is the shifted resonant frequency of resonator 1, and  $f_2$  is the shifted resonant frequency of resonator 2. The term  $f_{0_1}$  is the resonant frequency of resonator 1 in the absence of coupling, and  $f_{0_2}$

is the resonant frequency of resonator 2 in the absence of coupling. The coupling parameters,  $\alpha$ ,  $\beta$ , and  $D$  are found from the self and mutual energies as

$$\alpha_{12} = \frac{W_{m,12}}{\sqrt{W_{m,11}W_{m,22}}} \quad (3)$$

$$\beta_{12} = \frac{W_{e,12}}{\sqrt{W_{e,11}W_{e,22}}} \quad (4)$$

$$D = \sqrt{\frac{W_{m,22}}{W_{m,11}}} \quad (5)$$

where  $W_e$  denotes the electric energy and  $W_m$  denotes the magnetic energy. It should also be pointed out that the term  $Q$  in Equations (1) and (2) is the time dependent charge. This term serves as the generalized coordinate by which the Lagrangian is defined for metamaterial structures. The charge is assumed to be  $Q \sim |Q|e^{j\omega t}$ .

The self and mutual energies are calculated from the  $\mathbf{E}$  and  $\mathbf{H}$  fields along with the current and charge distributions obtained from full wave electromagnetic analysis. It has been suggested that image theory can be used to compute the coupling parameters in a waveguide based only on the current and charge distributions. Unfortunately, it is not always possible to successfully apply image theory, and inaccurate predictions of the resonant frequency may result. By using field terms, all electromagnetic interactions are considered, so accurate results are achieved regardless of the guiding structure. The electric and magnetic energies in terms of fields are written as

$$W_e = \frac{1}{2} \left[ \int_v \epsilon \mathbf{E} \cdot \mathbf{E} dv' + \epsilon \oint_s V \mathbf{E} \cdot \hat{\mathbf{a}}_n ds' \right] \quad (6)$$

$$W_m = \frac{1}{2} \left[ \int_v \mu \mathbf{H} \cdot \mathbf{H} dv' - \oint_s (\mathbf{A} \times \mathbf{H}) \cdot \hat{\mathbf{a}}_n ds' \right] \quad (7)$$

where the integration is taken over the area enclosing each resonant structure, and  $V$  and  $\mathbf{A}$  are the electric scalar potential and the magnetic vector potential respectively. Note that in some cases, the terms containing  $V$  and  $\mathbf{A}$  may be left out of Equations (6) and (7) as these terms fall off rather rapidly with distance from the source. For completeness, these terms remain in the equations.

To apply the Lagrangian formulation using the fields analysis discussed herein, the medium enclosing the resonant structure and the location where the second, coupled resonator would be placed are discretized into small segments indicated in Figure 1. The resonant structure is also discretized into small segments where the charge and current are assumed approximately uniform on each segment. The necessary data is calculated for each volume or surface and extracted for post processing. The energy equations become summations of Equations (6) & (7) and are written as

$$W_{e,pq} = \sum_{k_v=1}^{K_v} \frac{1}{2} \left[ \int_v \epsilon \mathbf{E}_{k_v}^p \cdot \mathbf{E}_{k_v}^q dv' \right] + \sum_{c=1}^C \sum_{k_s=1}^{K_s} \frac{1}{2} \left[ \epsilon \oint_s V_c^q \mathbf{E}_{k_s}^p \cdot \hat{\mathbf{a}}_n ds' \right] \quad (8)$$

$$W_{m,pq} = \sum_{k_v=1}^{K_v} \frac{1}{2} \left[ \int_v \mu \mathbf{H}_{k_v}^p \cdot \mathbf{H}_{k_v}^q dv' \right] - \sum_{c=1}^C \sum_{k_s=1}^{K_s} \frac{1}{2} \left[ \oint_s (\mathbf{A}_c^q \times \mathbf{H}_{k_s}^p) \cdot \hat{\mathbf{a}}_n ds' \right] \quad (9)$$

where the superscripts  $p$  and  $q$  indicate the fields generated by the corresponding resonator. The self energy is computed when  $p = q$ , and the mutual energy is computed when  $p \neq q$ . The subscripts,  $k_s$  and  $k_v$ , correspond to the respective surface or volume element for the discretized region surrounding the resonant structure. The subscript,  $c$ , corresponds to the respective discretized segment of the resonator.

It is clear from Equations (1)–(5) that manipulation of  $\alpha$  and  $\beta$ , or more specifically the mutual energies, can be used to tune the resonant frequency. One way to do this is by varying the distance,  $\Delta_X$ , between the resonant structures. The flow chart in Figure 2 illustrates the process for determining the resonant frequencies for two coupled resonators with variations in  $\Delta_X$ . The following list further clarifies the simulation and analysis procedure outlined in Figure 2:

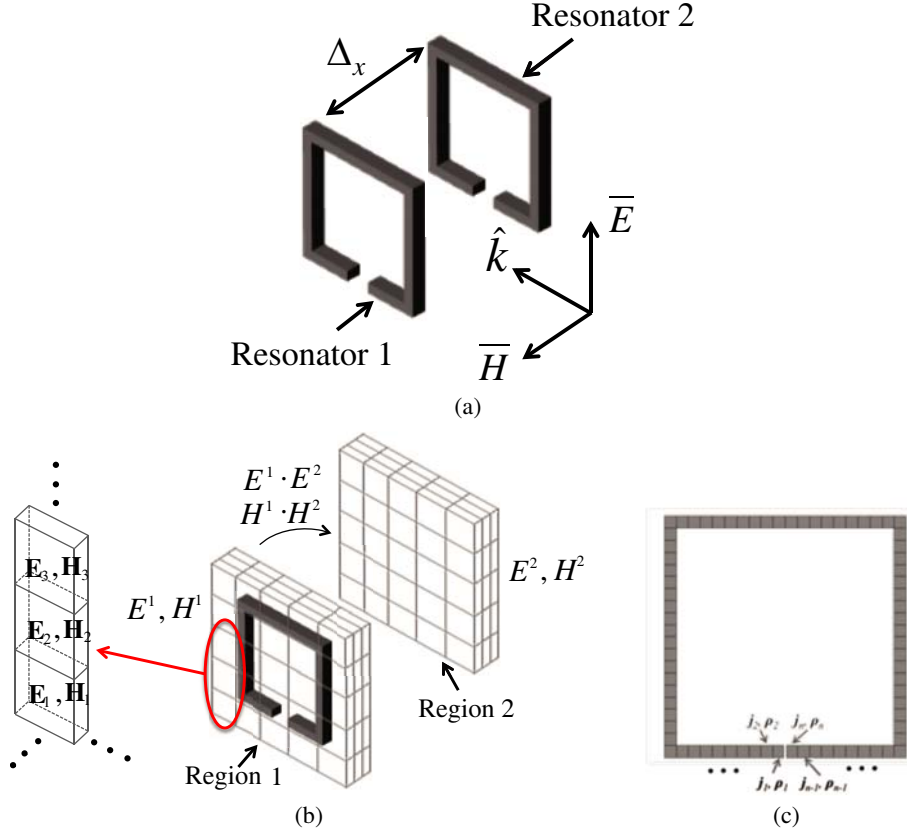


**Figure 1.** Two coupled split ring resonators (a) showing the alignment of the excitation field along with the direction of propagation. An illustration for the discretization enclosing a split ring resonator and coupled region (b) is also shown along with the discretization of a split ring resonator (c).

1. Simulate resonator 1 at  $f_{0_1}$  — resonator 1 is simulated in the operating environment at its resonant frequency without including resonator 2. The data generated by this simulation alone is used to compute the self energies  $W_{e,11}$  and  $W_{m,11}$ .
2. Discretize region 1 and extract field data for  $W_{e,11}$  and  $W_{m,11}$  — the region within the guiding structure that encloses resonator 1 and the resonator are discretized, and necessary data is extracted for Equations (8) and (9).
3. Simulate resonator 2 at  $f_{0_1}$  — resonator 2 is simulated in the operating environment at the resonant frequency of resonator 1. Resonator 1 is not included in this simulation. The simulation is performed at  $f_{0_1}$  because we need to know the amount of coupling (electric and magnetic energy) between resonators 1 and 2 at the frequency  $f_{0_1}$ . The coupling at  $f_{0_1}$  determines the impact to the resonant frequency  $f_{0_1}$ . The data generated in this simulation alone is used to compute the self energies  $W_{e,22}$  and  $W_{m,22}$ . The data generated in this simulation along with the data generated in step 1 is used to compute the mutual energies  $W_{e,12}$  and  $W_{m,12}$ .
4. Discretize region 2 and extract field data for  $W_{e,22}$  and  $W_{m,22}$  — the region enclosing resonator 2 and the resonator are discretized, and the necessary data is extracted for energy computations. The data generated by this simulation is all that is necessary to calculate the self energies  $W_{e,22}$  and  $W_{m,22}$ . Note that the volumetric discretization enclosing resonator 2 is performed to the same level as that for resonator 1, i.e., the same number of data points are used at the same relative positions. On the other hand, the discretizations of the two resonators may vary if the resonators vary in geometry.
5. Discretize region 1 and extract field data for  $W_{e,12}$  and  $W_{m,12}$  — in the full wave model for resonator 2, the region where resonator 1 would be placed relative to resonator 2 is discretized. The field

data generated by resonator 2 in the region that would enclose resonator 1 for the coupled scenario is extracted to compute the mutual energies. This data along with the data extracted in step 2 is used to compute the mutual energies.

6. Compute  $\alpha_{12}$ ,  $\beta_{12}$ ,  $D$  — use the extracted field data to compute the energies and the resulting coupling parameters.
7. Compute the shifted resonant frequency  $f_1$  — using the coupling parameters, compute the shift on  $f_{0_1}$  as a result of coupling.
8. Repeat steps 5–7 for changes in resonator separation distance,  $\Delta_X$  — repeat these steps as needed for various resonator spacings. Note that no full wave analysis is required following the simulations of steps 1 and 3. All other steps are field extraction and data processing.

For this investigation, the resonant structures are simulated using the finite element solver in HFSS to obtain the appropriate field data. MATLAB routines are used to perform the post processing and calculate the coupling parameters. Extraction of the field data requires a bit of scripting, but once the field data is extracted, the coupling terms and resonant frequency for a single value of  $\Delta_X$  are computed in less than one second on a 2.6 GHz Intel Core i7 processor with 8 GB of RAM. It is evident from Figure 2 that the Lagrangian design method is an iterative process to find the appropriate spacing for a desired resonant frequency. However, the speed with which each iteration is performed enables rapid convergence of a solution. Furthermore, this approach can be used as a rapid design tool to investigate the tunability or sensitivity of a particular set of resonators. One full wave simulation of two very simple split ring resonators at a single value of  $\Delta_X$  with the HFSS finite element method (FEM) solver uses a mesh size up to approximately 30,000 tetrahedra to capture the resonant behavior of the rings. The tetrahedra count can increase dramatically for multi-band solutions or resonators with complex geometries leading to lengthy simulations. A full set of analyses to evaluate many filtering positions could take considerable time and computing resources, and the Lagrangian approach provides a fast alternative. Furthermore, the data generated by the Lagrangian analysis can provide physical insight to the coupling mechanisms at work between coupled resonators. As an application example, the Lagrangian formulation is applied to the design of a WR-187 horn antenna with integrated notch filter.

### 3. HORN ANTENNA WITH COUPLED RESONATOR NOTCH FILTER

The analysis outlined in the previous section is applied here to realize a coupled resonator notch filter for operation in the WR-187 waveguide band. The dimensioned HFSS model for the horn antenna including the split ring resonator is shown in Figure 3. The horn antenna is designed according to [16] for approximately 15 dBi of gain at a center frequency of 4.75 GHz. The split ring resonator is designed for a resonant frequency of approximately 5.8 GHz in the absence of coupling. Split rings are selected as the filtering elements due in part to the simplicity in design and fabrication. These resonators also give very controllable filtering that exhibits little interaction with the incident field outside of the dominant mode resonance location. This generally results in a very clean notch response with good performance outside of the notch band.

In this paper, two coupled split rings are considered in two distinct orientations, broadside coupled and gap coupled, as shown in Figure 4(b). The rings are configured with their axes aligned so that there is no shifting between rings in the direction of propagation. The rings are varied by the amount,  $\Delta_X$ , only in the direction of the  $\mathbf{H}$ -field transverse to propagation. The distance  $\Delta_X$  is swept over a range of values initially to investigate tunability between the two configurations. In this case, the resonators are identical so  $f_{0_1} = f_{0_2}$ ,  $W_{m,11} = W_{m,22}$ ,  $W_{e,11} = W_{e,22}$ , and  $Q_1 = Q_2$ . The coupling parameters reduce to

$$\alpha = \frac{W_{m,12}}{W_{m,11}} \quad (10)$$

$$\beta = \frac{W_{e,12}}{W_{e,11}} \quad (11)$$

$$D = 1 \quad (12)$$

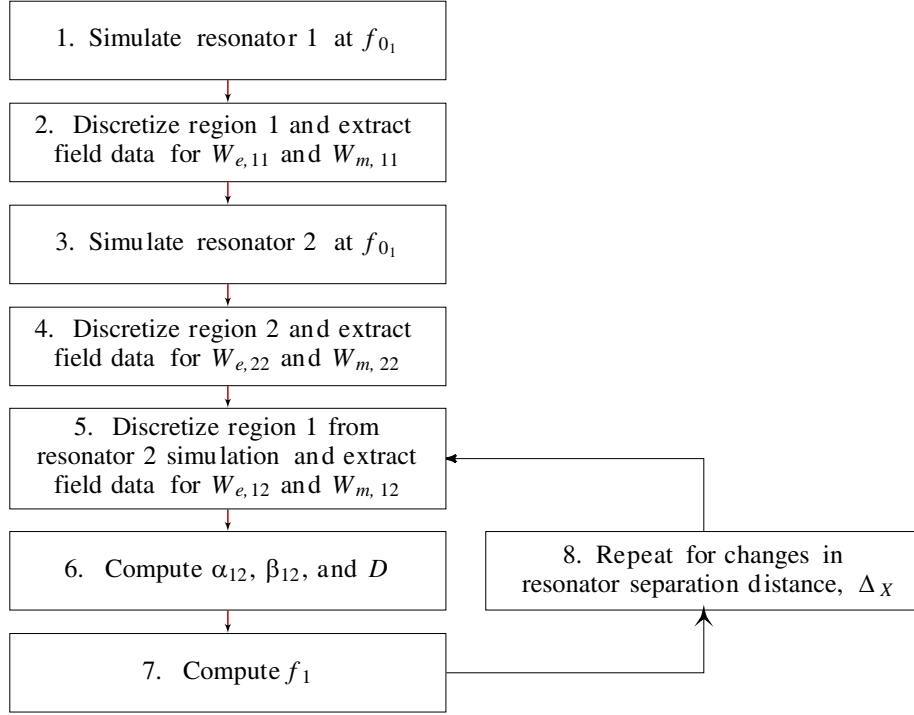


**Figure 2.** Flow chart illustrating the process to calculate resonant frequencies for coupled metamaterial structures using the Lagrangian method.

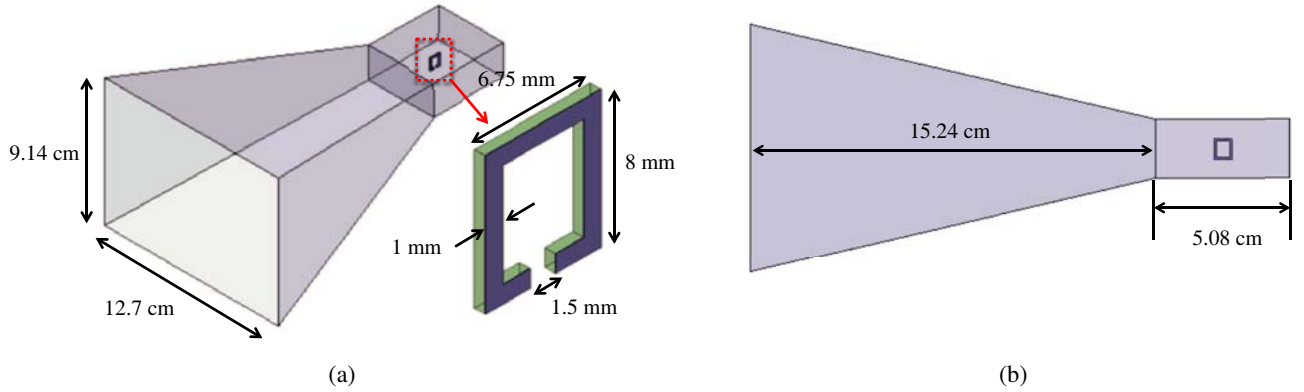


**Figure 3.** Horn antenna with SRR integrated into the feed portion. The isometric view (a) illustrates the horn and split ring dimensions and the side view (b) shows the length of the horn and the feed section. The split ring resonator is modeled on  $(1/32)$ " FR-4 with 1/2 oz. cladding. The SRR is positioned centrally in the waveguide 2.2 cm from the throat of the horn.

and the system of resonators exhibits a resonant frequency given by

$$f_r = f_0 \sqrt{\frac{1 + \beta}{1 + \alpha}} \quad (13)$$

where  $f_r$  is the operating frequency of the coupled resonator notch filter. This solution is known as the symmetric coupling mode. As shown in [12] the other solution that satisfies the equations of motion for the system of identical resonators is the asymmetric mode where  $Q_1 = -Q_2$ . This solution is the result of resonance splitting and occurs when the current and charge are  $180^\circ$  out of phase between the two rings. This mode is generally only present when the rings are shifted relative to one another in

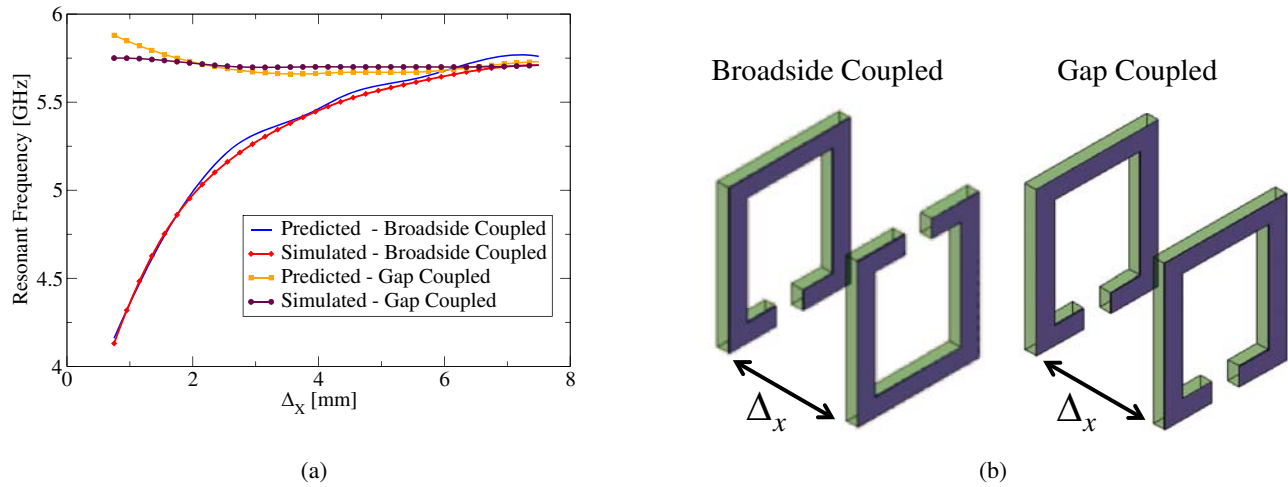


**Figure 4.** Predicted and simulated resonant frequencies for broadside coupled rings and gap coupled rings with various spacing,  $\Delta_x$ , (a) and illustration for broadside coupled and gap coupled split ring orientations (b).

the direction of propagation. As opposed to the approach in [11], the rings are allowed to shift only transverse to propagation, and the asymmetric mode is avoided altogether eliminating the possibility of unwanted resonances outside of the intended operating band of the filter.

To determine the coupled resonant frequencies, individual rings are simulated as outlined in the previous section, and the necessary data is extracted for post processing. Following the numerical analysis, the coupling parameters in Equations (10) and (11) are calculated in a matter of seconds as described in the previous section, and the resonant frequencies are determined according to Equation (13). In this case, the operating environment for numerical analysis is the feed portion of the horn antenna pictured in Figure 3 where both rings are simulated individually in the center of the waveguide. By simulating both rings in the center of the guide, we ignore the amplitude variation of the excitation field due to the waveguide field distribution. We find that this provides sufficiently accurate results. The Lagrangian predicted resonant frequencies are plotted in Figure 4(a) over the range of  $\Delta_x$ . The coupled rings in each configuration are also simulated in HFSS for comparison. For numerical analyses, the horn antenna including the filtering element is modeled with the FEM solver in HFSS and uses mesh sizes ranging from approximately 15,000 to 30,000 tetrahedra. The walls of the waveguide and horn along with the metal of the resonators are modeled as perfect electric conductor (PEC). The dielectric of the SRRs is modeled as FR-4. All other space within the solution domain is modeled as vacuum, and the solution domain is enclosed inside of a box whose walls are separated from the antenna by  $\lambda_0/4$  at 3.5 GHz. A radiation boundary is assigned to the faces of the box enclosing the solution domain. The end of the waveguide opposite to the opening of the horn is covered with a waveport to provide the excitation. Predicted resonant frequencies correlate very well with simulated data for distance variations in both split ring orientations. This illustrates the accuracy of the Lagrangian solution. It is also apparent from Figure 4 that broadside coupled rings offer much more tuning bandwidth than gap coupled rings.

The antenna performance is specifically investigated in HFSS for the rings in each configuration with separation distances,  $\Delta_x$ , of 0.6 mm, 1.4 mm and 6.5 mm. These values for  $\Delta_x$  give resonant frequencies of approximately 3.9 GHz, 4.6 GHz, and 5.7 GHz for the broadside coupled rings based on the Lagrangian analysis. The simulated return loss and boresight gain data for the gap coupled rings is shown in Figure 5 where the predicted resonant frequencies are confirmed. Even with significant variation in the distance between the rings, there is very little variation in the resonant frequency. The gap coupled filter with rings spaced 0.6 mm, 1.4 mm, and 6.5 mm gives notch frequencies at 5.75 GHz, 5.74 GHz, and 5.72 GHz. The bandwidth for the three filter spacings varies from approximately 110–

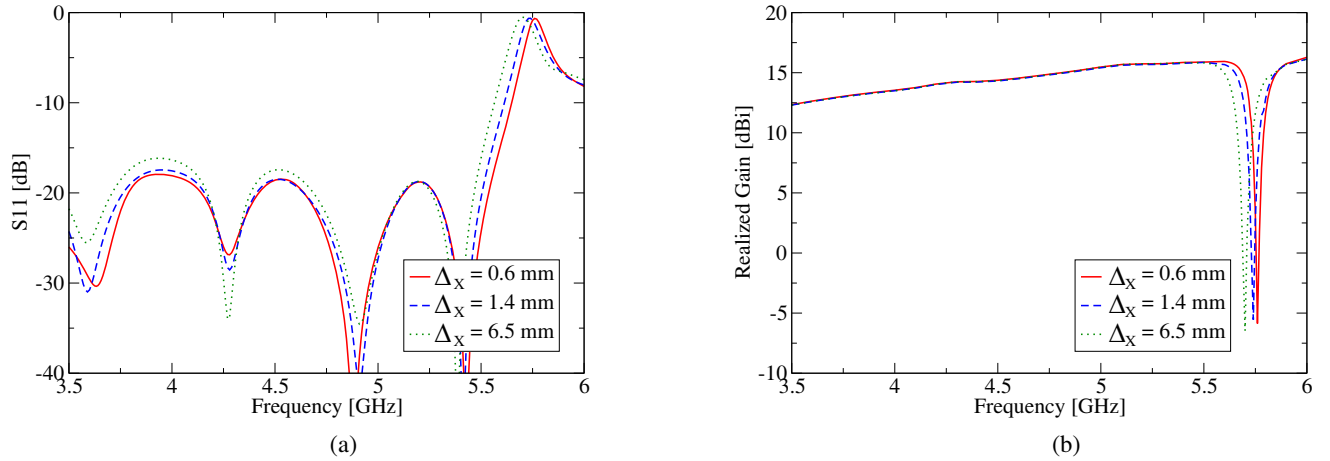


**Figure 5.** Simulated return loss (a) and normalized gain (b) for the horn antenna with three fixed filters of gap coupled split rings with  $\Delta_x$  set to 0.6 mm, 1.4 mm, and 6.5 mm.

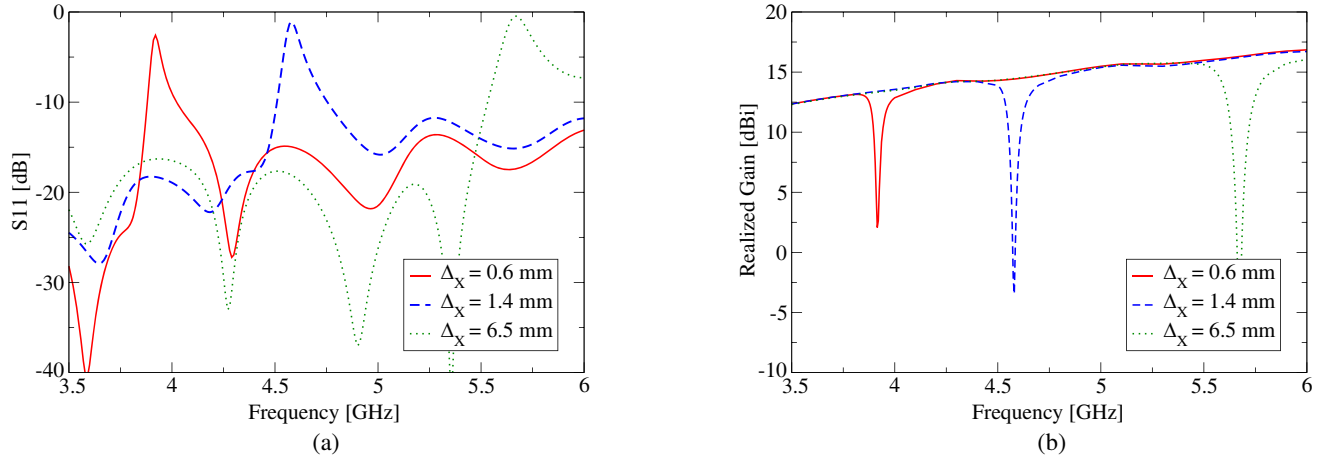


**Figure 6.** Simulated return loss (a) and normalized gain (b) for the horn antenna with three fixed filters of broadside coupled split rings with  $\Delta_x$  set to 0.6 mm, 1.4 mm, and 6.5 mm.

150 MHz determined by where the boresight gain is reduced by 3 dBi.

The broadside coupled rings, on the other hand, exhibit considerable tunability as indicated by the return loss and gain shown in Figure 6. The broadside coupled filter with rings spaced 0.6 mm, 1.4 mm, and 6.5 mm exhibits notch frequencies at 3.92 GHz, 4.58 GHz, and 5.68 GHz confirming the predicted resonances. The bandwidth for the three filter spacings varies from approximately 40 MHz at the lowest operating frequency to approximately 150 MHz at the highest operating frequency. Due to the significant tunability of the broadside coupled rings compared to the gap coupled rings, broadside coupling is the obvious choice for reconfigurable notch filter solutions. A gap coupled approach would only complicate the fabrication process while offering little tuning advantage.

Tremendous tuning range is achieved with the broadside coupled configuration, but we also observe a reduction in the amount of rejection by the filter at lower frequencies. This is due to the nature of the coupling required for large shifts in the resonant frequency. The physical explanation for the large tuning range in broadside coupled split rings can be found by looking at the charge and current distributions. The gaps are oriented on opposite sides of the rings, and the current flow on the two rings is in the same direction. Therefore, the electric potentials in the gaps of the two rings are oriented in opposite directions as illustrated in Figure 7. What results is an odd-mode type of response where the

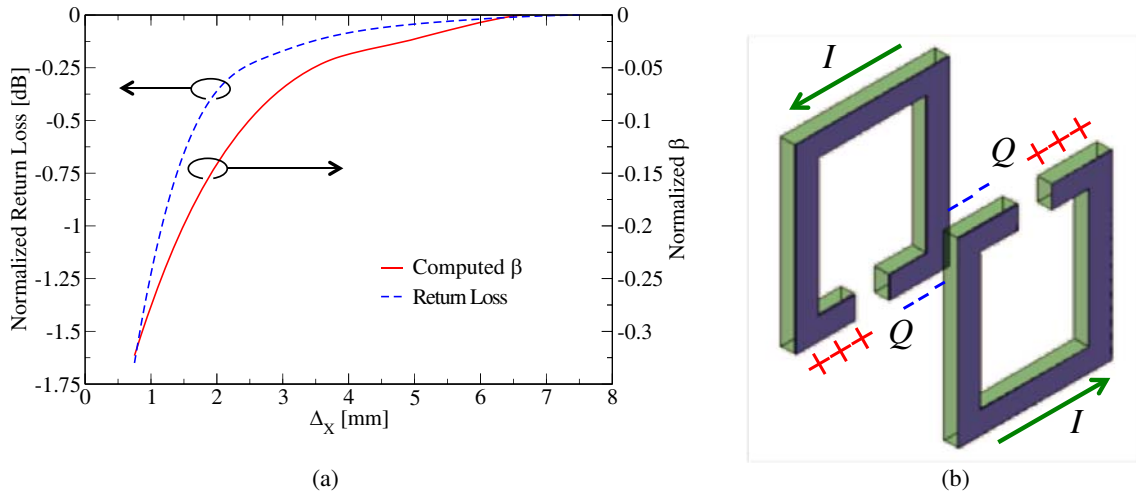


**Figure 7.** Plot of normalized electrical coupling parameter,  $\beta$ , vs separation distance and simulated return loss in dB vs separation distance for broadside coupled rings (a) and illustration of current and charge at resonance for broadside coupled split rings (b).

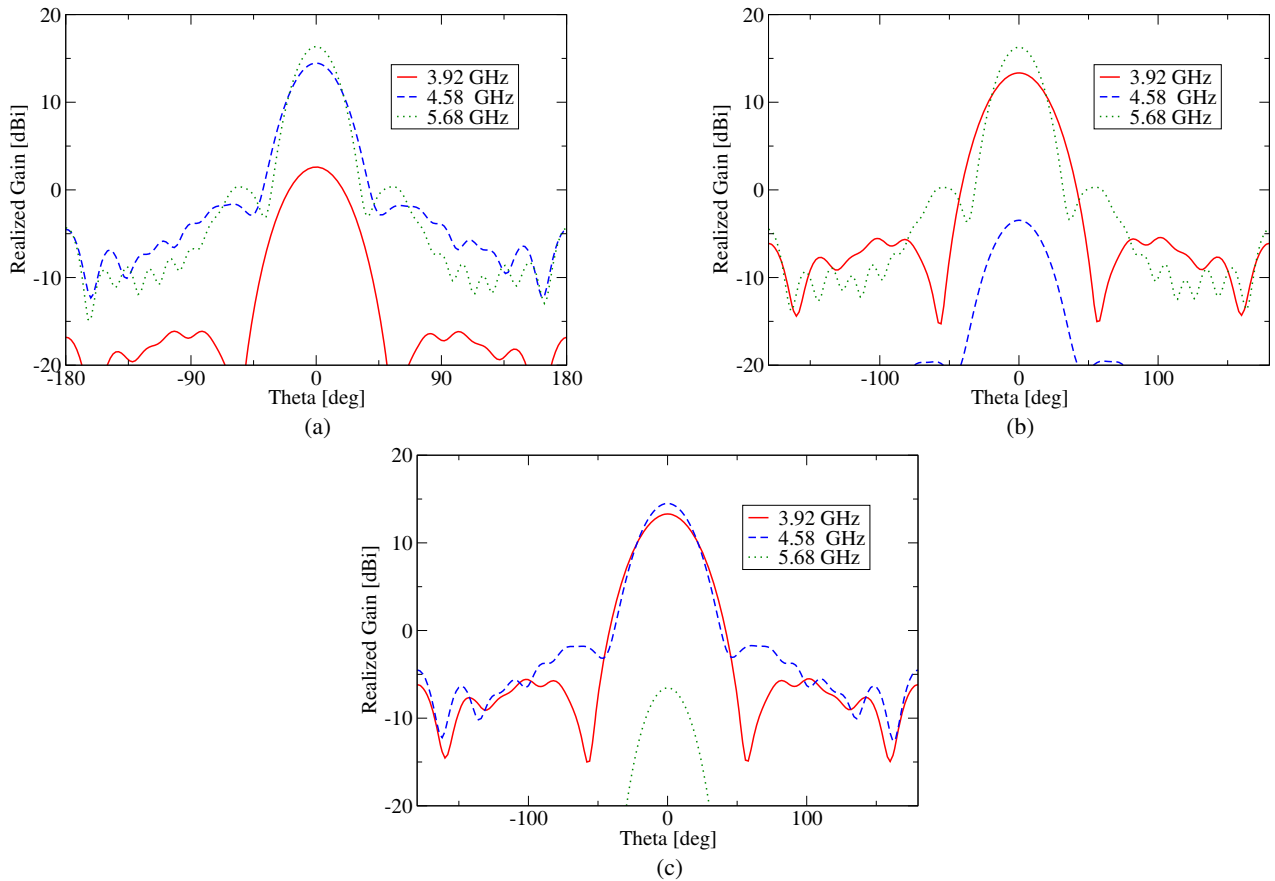


**Figure 8.** Simulated pattern data for the horn antenna integrated with the broadside coupled ring notch filter. Patterns were plotted at 3.92 GHz, 4.58 GHz, and 5.68 GHz for the three different filtering configurations with  $\Delta_x = 0.6$  mm (a),  $\Delta_x = 1.4$  mm (b), and  $\Delta_x = 6.5$  mm (c).

electric fields between the two rings partially cancel reducing the scattered electric field and allowing some energy to pass through the filter. This effect can also be observed through investigation of the electrical coupling parameter,  $\beta$ , from Equation (13). Figure 7(a) shows a plot of the normalized return loss along with the calculated value for  $\beta$ . The negative value for  $\beta$  comes as a result of the charge distributions outlined in Figure 7(b), and the magnitude of  $\beta$  reveals the amount of electrical coupling between the resonators. The higher the magnitude of  $\beta$ , the more electrical coupling there is between the resonators. Although the magnitude of beta is relatively high for closely spaced resonators, there is destructive interference that allows some energy through the filter. We find that this trend in  $\beta$  corresponds very well to the trend in return loss over the values of  $\Delta_x$ . Fortunately, even with the reduction in reflection for closely spaced resonators, we observe approximately 12 dB of filtering in the center of the notch band at 3.92 GHz.

The far field patterns for the broadside coupled rings are also investigated numerically to ensure minimal perturbation outside of the operating frequency of the notch filter. It is found that the patterns are impacted insignificantly outside of the operating band of the filter as indicated by the patterns in Figure 8 and the gain in Figure 6(b). As a result, the filtering element can be placed very close to the throat of the horn antenna for an integrated, compact solution. However, it should be noted that shifting the resonators closer to the throat of the antenna can cause slight shifts in the resonant frequency. Along the same lines, shifting the rings transverse to propagation can also cause shifts in the resonant frequency. Placement of the rings off-center in the waveguide along the direction of the **H**-field can further cause less rejection by the filter as the rings are shifted out of the region of the strongest **E**-fields. Movement of the rings out into the throat of the horn also results in less rejection by the filter; however, this could be overcome by redesigning the rings to occupy more physical space inside the throat of the horn.

#### 4. PROTOTYPE FABRICATION AND EXPERIMENTAL RESULTS

A proof-of-concept horn antenna with wide tuning range is fabricated with fixed inserts of broadside coupled split ring resonators to confirm the design approach. The mechanical structure for the horn antenna is 3D printed out of ABS plastic using a Makerbot desktop 3D printer with design dimensions corresponding to those in Figure 3. The inner portions of the antenna are lined with copper foil, and the antenna is bolted together to make solid electrical contact. The fabricated structure is pictured in Figure 9.

The split rings are milled out of single-sided (1/32)" FR-4 pcb board with 1/2 oz. copper cladding. The rings are milled with dimensions corresponding to those in Figure 3(a) with FR-4 supports left on either side of the ring as shown in Figure 9(d). The supports are used to position the rings in extruded polystyrene foam as shown in Figure 9(a) where digital calipers are used to generate the appropriate spacings for each set. As discussed in the previous section, the rings are spaced at approximately 0.6 mm, 1.4 mm, and 6.5 mm to generate notch bands at approximately 3.9 GHz, 4.6 GHz, and 5.7 GHz respectively.

**Table 1.** Simulated vs. measured resonant frequency and bandwidth for three broadside coupled filters.

$\Delta_x$	Simulated		Measured	
	$f_r$	Bandwidth	$f_r$	Bandwidth
0.6 mm	3.92 GHz	40 MHz	3.86 GHz	35 MHz
1.4 mm	4.58 GHz	70 MHz	4.53 GHz	45 MHz
6.5 mm	5.68 GHz	150 MHz	5.65 GHz	100 MHz

The return loss and power transmission are measured for the horn antenna with the three filter inserts, and the results are plotted in Figure 10 along with the simulated results for comparison. The return loss is measured using an Anritsu 37297D vector network analyzer, and the power transmission is measured using a FieldFox N9938A spectrum analyzer. The horn antenna with coupled resonator

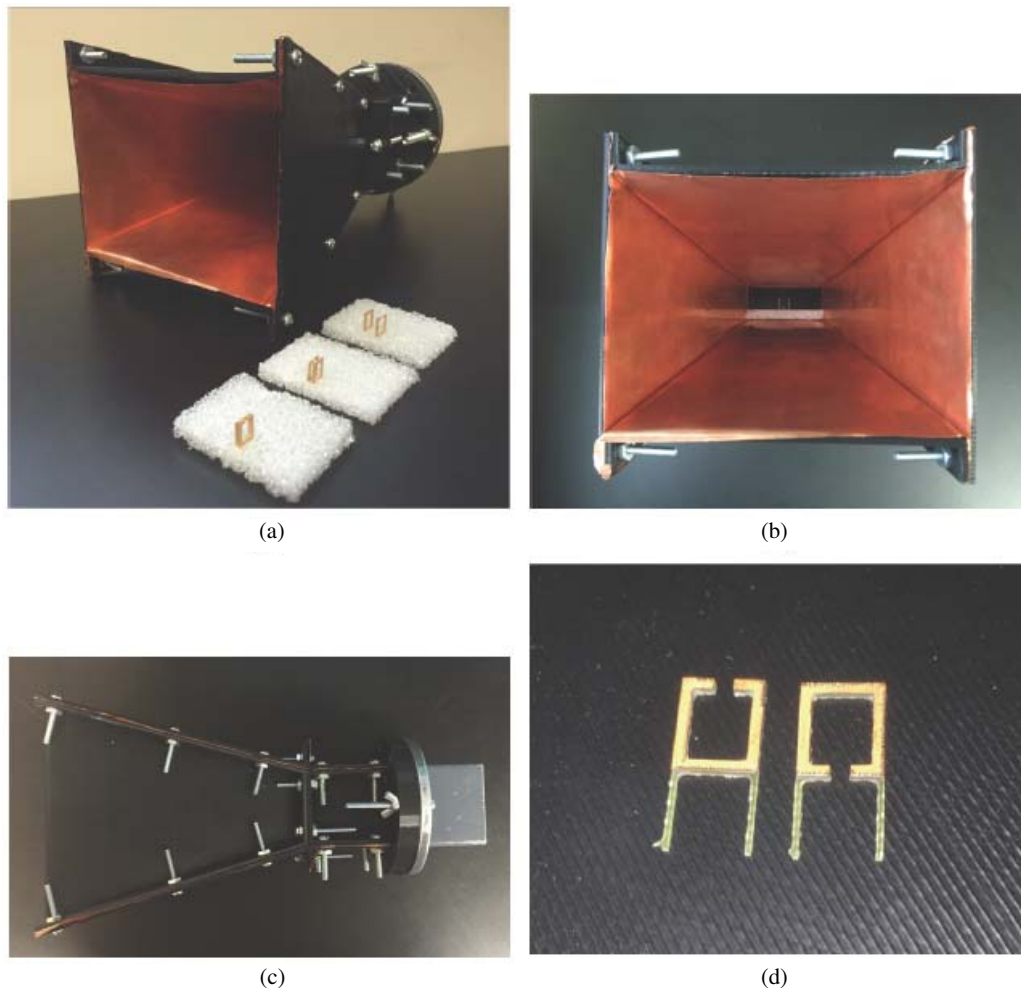


**Figure 9.** Isometric view of fabricated horn antenna with coupled resonator filters (a), front view of horn antenna with filter inserted into feed (b), top view of fabricated horn antenna (c), and fabricated split ring resonators (d).

filter is used as the source antenna while an Aaronia HyperLog 6080 log periodic antenna is used as the receive antenna. The measured return loss and power transmission agree well with simulated data confirming the design approach and illustrating the wide tuning bandwidth for broadside coupled split rings. It is found that the horn antenna does not operate quite as low in frequency as indicated by simulations, but this is likely due to small tolerances in the 3D printed structures resulting in a slightly undersized waveguide with a slightly higher cutoff frequency for the dominant  $TE_{10}$  mode. Fortunately, there is no distinct impact to the filtering as the result of a slightly undersized waveguide. There are very minor shifts in the operating frequencies and 3 dB bandwidths of the three measured filters compared to simulation. The simulated and measured data is compared in Table 1. The slight shifts in the resonant frequencies and bandwidths are the result of fabrication and positioning tolerances between the rings. For a production solution, the rings would be precisely positioned using low loss dielectric foam to ensure repeatability. We also observe less gain reduction for the measured filter in the notch bands compared to simulated results. This is partly due to slightly less rejection by the fabricated filter as a result of the rings being positioned slightly off-center in the waveguide. This is also likely due to a small amount of noise in the measurement setup making it difficult to get very clean measurements for power transmission in the notch bands. Nonetheless, effective filtering is demonstrated, and the design approach is confirmed.

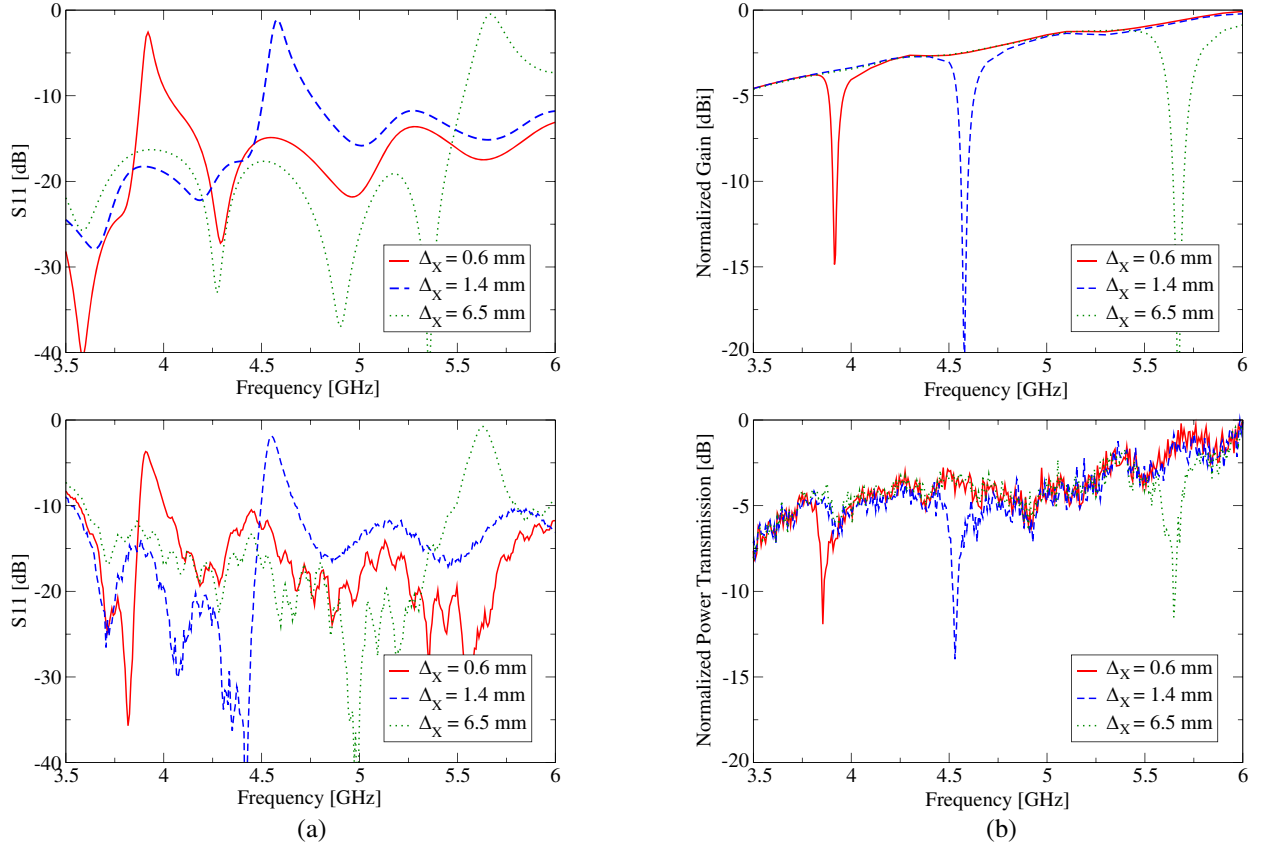


**Figure 10.** Simulated (top) and measured (bottom) return loss (a) along with normalized gain and power transmission, respectively (b) for the horn antenna with three fixed filters of broadside coupled rings with  $\Delta_x$  set to 0.6 mm, 1.4 mm, and 6.5 mm.

## 5. CONCLUSION

In this paper, the Lagrangian formulation for metamaterials is presented as a fast and accurate design approach for guided wave notch filters. Using this approach, many filtering configurations can be investigated in a matter of seconds where full-wave analysis could be computationally intensive and time consuming. The formulation is presented using a fields approach making it suitable for the design of a broad class of guided wave filters based on coupled metamaterials. A horn antenna with integrated notch filter is presented where the filter could be reconfigured to operate over a very wide bandwidth. It is shown that broadside coupled rings offer much more tunability than gap coupled rings. The rejection of the filter over the tuning range is also addressed by investigation of the coupled filter electrical response. This electrically small and versatile filtering approach can be implemented in a wide range of guided wave devices, and tuning by mechanical means could be implemented for dynamic tuning.

## REFERENCES

1. Veselago, V. G., “The electrodynamics of substances with simultaneously negative values of permittivity and permeability,” *Sov. Phys. Uspekhi*, Vol. 10, 509–514, 1968.
2. Pendry, J. B., “Negative refraction makes a perfect lens,” *Phys. Rev. Lett.*, Vol. 85, 3966, 2000.
3. Shelby, R. A., D. R. Smith, and S. Schultz, “Experimental verification of negative index of refraction,” *Science*, Vol. 292, 77–79, 2001.

4. Ziolkowski, R. W., "Design, fabrication, and testing of double negative metamaterials," *IEEE Trans. Antennas Propag.*, Vol. 51, No. 7, 1516–1529, 2003.
5. Solymar, L. and E. Shamonina, *Waves in Metamaterials*, Oxford University Press, New York, 2009.
6. Palandoken, M., *Metamaterial-based Compact Filter Design*, Metamaterial, X. Jiang (Ed.), InTech, DOI: 10.5772/35853, 2012.
7. Fallahzadeh, S., H. Bahrami, and M. Tayarani, "A novel dual-band bandstop waveguide filter using split ring resonators," *Progress In Electromagnetics Research Letters*, Vol. 12, 133–139, 2009.
8. Gangaraj, S. H. and M. Tayarani, "A novel bandstop resonator in waveguide and its application for suppressing the spurious responses with new advantages to typical resonators," *PIERS Proceedings*, 533–537, Suzhou, China, September 12–16, 2011.
9. Barbuto, M., F. Trotta, F. Bilotti, and A. Toscano, "Horn antennas with integrated notch filters," *IEEE Trans. Antennas Propag.*, Vol. 63, No. 2, 781–785, 2015.
10. Barbuto, M., F. Trotta, F. Bilotti, and A. Toscano, "Varying the operation bandwidth of metamaterial-inspired filtering modules for horn antennas," *Progress In Electromagnetics Research C*, Vol. 58, 61–68, 2015.
11. Shehan, J. W. and R. S. Adams, "X-band horn antenna with integrated tunable notch filter," *2015 IEEE International Symposium on Antennas and Propagation (APSURSI)*, 2213–2214, 2015.
12. Powell, D. A., M. Lapine, M. V. Gorkunov, I. V. Shadrivov, and Y. S. Kivshar, "Metamaterial tuning by manipulation of near-field interactions," *Phys. Rev. B*, Vol. 82, 155128, 2010.
13. Powell, D. A., K. Hannam, I. V. Shadrivov, and Y. S. Kivshar, "Near-field interaction of twisted split-ring resonators," *Phys. Rev. B*, Vol. 83, 235420, 2011.
14. Withayachumnankul, W., C. Fumeaux, and D. Abbot, "Near-field interactions in electric inductive-capacitive resonators for metamaterials," *Journal of Phys. D: Applied Phys.*, Vol. 45, No. 48, 485101, 2012.
15. Haus, H. A. and W. Huang, "Coupled-mode theory," *Proceedings of the IEEE*, Vol. 79, No. 10, 1505–1518, 1991.
16. Balanis, C. A., *Antenna Theory: Analysis and Design*, 3rd edition, John Wiley & Sons, New Jersey, 2005.